

Intrinsically disordered nuclear pore proteins show ideal-polymer morphologies and dynamics

Luke K. Davis,^{1,2,3} Ian J. Ford,^{1,2} Anđela Šarić,^{2,3,*} and Bart W. Hoogenboom^{1,2,3,†}

¹*London Centre for Nanotechnology, University College London,
London WC1H 0AH, United Kingdom*

²*Department of Physics and Astronomy,
University College London, London WC1E 6BT, United Kingdom*

³*Institute for the Physics of Living Systems,
University College London, London WC1E 6BT, United Kingdom*

(Dated: March 8, 2019)

Abstract

In the nuclear pore complex (NPC), intrinsically disordered nuclear pore proteins (FG nups) form a selective barrier for transport into and out of the cell nucleus, in a way that remains poorly understood. The collective FG nup behaviour has long been conceptualized either as a polymer brush, dominated by entropic and excluded-volume (repulsive) interactions, or as a hydrogel, dominated by cohesive (attractive) interactions between FG nups. Here we compare mesoscale computational simulations with experimental data to demonstrate that FG nups are at the crossover point between these two regimes. Specifically, we find that repulsive and attractive interactions are balanced, resulting in morphologies and dynamics that are close to those of ideal polymer chains, where repulsion and attraction are absent. We demonstrate that this yields sufficient cohesion to seal the transport barrier, and yet maintains fast dynamics at the molecular scale, permitting the rapid FG nup rearrangements needed for transport events.

* a.saric@ucl.ac.uk

† b.hoogenboom@ucl.ac.uk

INTRODUCTION

Nuclear pore complexes (NPCs) penetrate the nuclear envelope in eukaryotic cells, controlling macromolecular transport between the nucleus and cytoplasm. The NPC enables small ($\lesssim 5$ nm in size) molecules to cross the nuclear envelope, but hinders the transport of larger macromolecules [1–3]. Larger macromolecular cargoes, however, can diffuse through the NPC if they are bound to nuclear transport receptors that have an affinity to the transport/permeability barrier. Remarkably, the NPC maintains the transport barrier while thousands of cargoes shuttle in and out of the cell nucleus per second [4]. This permeability barrier consists of proteins (nucleoporins) that are rich in phenylalanine (F) and glycine (G) repeats (hence called FG nups, for FG nucleoporins) and that are grafted to the inner wall of the NPC transport channel. These hydrophobic domains grant the FG nups cohesive properties, which may be counterbalanced by charged amino acids in hydrophilic spacer regions [5]. FG nups are natively unfolded proteins that arrange in disordered configurations [6], causing them to behave as flexible polymers [7].

For a long time, there have been conflicting views on the dominant interactions pervading FG nup assemblies, and these views continue to define the interpretation of experimental data. On one hand, repulsive interactions have been postulated to result in entropic polymer-brush behaviour of FG nups [8–10]. On the other hand, cohesive (*i.e.*, attractive) interactions can cause FG nups to form hydrogels *in vitro* [4, 11, 12]. We emphasize that these views represent two extreme regimes of polymer behaviour, and that the combined effects of repulsion, cohesion, grafting, and nanopore confinement lead to a rich landscape of possible polymer behaviour [13–16].

Recently, more nuanced views regarding FG nup interactions have emerged, substantiated by computational models of FG nups at different levels of coarse graining. By defining FG nups down to their amino acid composition, such models can relate, e.g., FG nup behaviour to their chemical composition and explore the effects of mutations [17, 18], with the important caveat that the results critically depend on parameter settings in a vast parameter space. Complementarily, at a coarser (“mesoscale”) level, FG nups have been modelled as homogeneous polymers with one essential interaction parameter [19, 20]. This approach facilitates the exploration of the relevant parameter space and the investigation into general aspects of polymer behaviour, at the cost of losing submolecular detail. Importantly, key

functional properties of FG nups have been reproduced by these models, strongly suggesting that NPC transport functionality may be generically understood in terms of mesoscale polymer physics. These studies have also indicated that FG nup assemblies display aspects of both entropic and cohesive physical behaviour.

Here we use mesoscale simulations to elucidate the relationship between repulsive and cohesive FG nup interactions. We incorporate experimental data on 27 different purified FG domains, that are either isolated or those that are grafted at physiological densities (FG nup assemblies), with *in vitro* morphologies as determined in 3 different laboratories [5, 9, 20–22]. We assess how the experimental morphologies compare with computational predictions on polymer behaviour from assemblies containing repulsive, cohesive, and completely non-interacting (“ideal”) polymers. We investigate how these behaviours translate into the static and dynamic properties of polymers in a context that is relevant to NPC transport functionality.

RESULTS

Morphologies of FG nups match predictions for ideal polymers

We model FG nups as freely jointed polymers consisting of N identical beads where one bead, with a diameter and bond length of 0.76 nm, represents two amino acids (Figure 1a). This choice in polymer model yields a predicted persistence length (0.38 nm) that agrees with experimental data on FG nups and other disordered polypeptide chains [23, 24], and approaches the excluded-volume of an FG nup (overestimating it by $\sim 20\%$ on average, see Table S1). FG nup excluded-volume (repulsive) and cohesive (attractive) interactions are modelled through a short-ranged pair potential with a minimum value of ϵ_{pp} , which is a measure of the cohesion strength between polymer beads (Figure S1a). Thus defined, ϵ_{pp} is a phenomenological parameter to capture the general cohesive properties of FG nups, with the appropriate parameterization also depending on the shape and range of the pair potential. In the range of ϵ_{pp} that we explore here ($0.0 k_B T \leq \epsilon_{pp} \leq 1.0 k_B T$), we find a dissociation constant of $K_D \sim 0.1$ M between two beads, implying that the affinity between individual beads is weak (see Figure S1b and Methods). To determine the physiologically relevant range of ϵ_{pp} , we computed hydrodynamic (Stokes) radii, R_S , from molecular dynamics (MD)

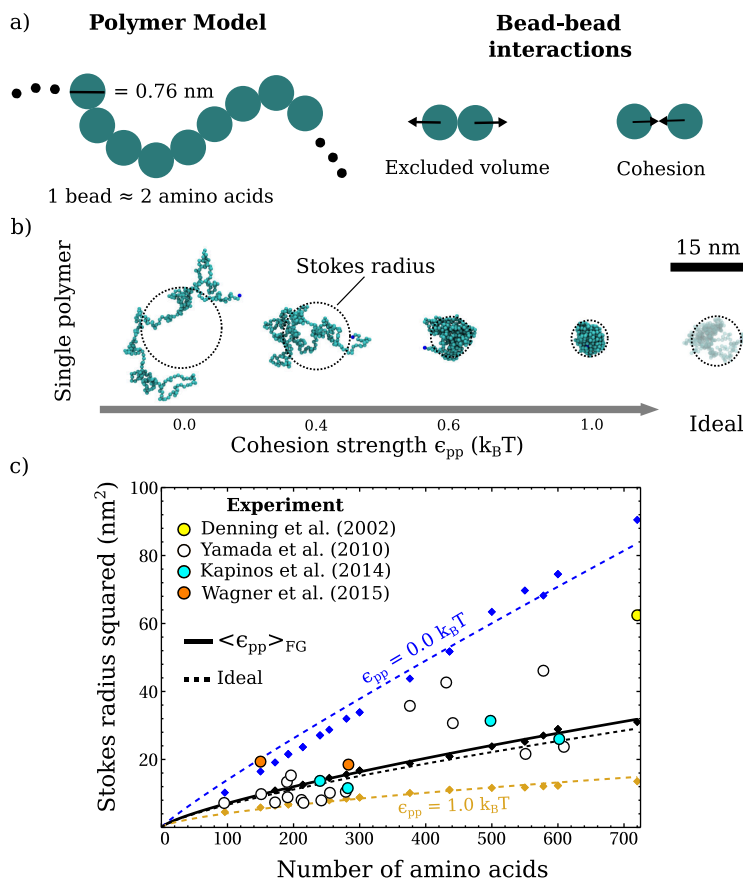


FIG. 1. Single-molecule parametrization of the polymer model by comparison with experimental Stokes radii [5, 9, 21, 22]. **a)** Illustration of the polymer model (MD) where FG nups are represented as beads on a chain, connected by stiff harmonic springs. Beads experience excluded-volume and cohesive interactions. **b)** MD snapshots of a polymer ($N = 300$ beads) as a function of the bead-bead cohesion strength ϵ_{pp} , alongside a polymer with no cohesion and no excluded-volume (“ideal”). The shown Stokes radius is calculated from an ensemble of equilibrated conformations. **c)** Experimental Stokes radii (circles) plotted for FG nup domains of different lengths (number of amino acids, see Table S1), compared with predictions of the polymer model (diamonds) alongside power law fits of the simulation data (solid and dotted lines). The black dotted lines (“Ideal”) represents the prediction for the case when excluded-volume and cohesive interactions are both nullified.

simulations of single polymers for various ϵ_{pp} (see Methods), and compared the results with experimental data on a wide range of single FG nup constructs [5, 9, 21, 22], similar to previous approaches [25] (see Table S1 for results). Qualitatively, at $\epsilon_{pp} = 0.0$ k_BT (no cohesion) a polymer is in a swollen state; for $0.0 < \epsilon_{pp} < 1.0$ k_BT polymers adopt morphologies that

become increasingly compact with increasing ϵ_{pp} ; and at $\epsilon_{pp} = 1.0 k_B T$ (“high cohesion”) a polymer forms a tight ball-like morphology (Figure 1b). A polymer with no excluded-volume interactions and no cohesive interactions between its beads, henceforward defined as an ideal polymer, acquires morphologies with sizes lying between that of a polymer with no and high cohesion (with excluded-volume).

Plotting Stokes radius squared, R_S^2 , against polymer length, we observe that 96% of the experimental data points fall within the simulation data calculated for no cohesion and for high cohesion (Figure 1c). Next, we determined the ϵ_{pp} values that yielded best matches between computational and experimental Stokes radii for the individual FG nups (Table S1). The average of these ϵ_{pp} values yields $\langle \epsilon_{pp} \rangle_{FG} = 0.5 \pm 0.2 k_B T$ (mean \pm standard deviation). Remarkably the data points for polymers with cohesion strength $\langle \epsilon_{pp} \rangle_{FG}$ coincide with the data for ideal polymers, in which all excluded-volume and cohesive interactions have been nullified (Figure 1c). This is a manifestation of polymers showing ideal polymer behaviour that typically occurs at Θ -point conditions [26]. For polymers with cohesion strength $\langle \epsilon_{pp} \rangle_{FG}$ and for ideal polymers we observe that R_S is roughly equal to the radius of gyration R_G , in agreement with data on intrinsically disordered proteins (see Figure S2) [27, 28]. We also note that R_S , for ideal polymers and polymers with no cohesion strength ($\epsilon_{pp} = 0.0 k_B T$), scales with the number of amino acids with an exponent ν that is slightly less than the scaling exponent for R_G , as is known for finite length polymers [29]; and that the experimental R_S scales with the number of amino acids with scaling exponent $\nu = 0.5 \pm 0.2$ (see Table S2).

Generally, to match the experimental data, the FG nup swelling due to excluded-volume interactions (Figure 1b) needs to be counteracted by intramolecular cohesion. As a consequence, overestimates of excluded-volume lead to larger ϵ_{pp} values. Nevertheless, and importantly, we observe that the match between the mean FG nup, $\langle \epsilon_{pp} \rangle_{FG}$, behaviour and ideal polymer behaviour is robust against the choice of model: using a model (with a bead size of 0.57 nm) that underestimates the excluded-volume and persistence length of FG nups, we find a smaller $\langle \epsilon_{pp} \rangle_{FG} = 0.26 \pm 0.06 k_B T$, yet for this $\langle \epsilon_{pp} \rangle_{FG}$ we still observe an excellent match with the ideal polymer prediction (Figure S2). Specific cases of significantly larger ϵ_{pp} could be correlated with larger overestimates of the excluded-volume in our simulations (Figure S3). In fact, variations in excluded-volume of the proteins (as compared with the polymer model) could account for apparent differences in FG nup extension/collapse that were previously attributed to differences in charged/polar and hydrophobic amino-acid

contents of different FG nups (Figure S3) [5].

FG nup assemblies show large morphological change in the physiologically relevant parameter range

In addition to the single-molecule parameterization, we also tested against experimental data on assemblies of FG nups that are grafted, at physiologically relevant densities, onto a planar surface (polymer films) [9, 20, 22]. MD simulations (Figure 2a) for $\langle\epsilon_{pp}\rangle_{FG} = 0.5 \pm 0.2 k_B T$ yield FG nup film thicknesses (Figure 2b, green shading) that are in agreement with the experimental data (Figure S4), with the exception of three data points. One data point (Nup214, blue symbol, 282 amino acids) has a film thickness that is less than the experimental Stokes radius and another data point (Nup62, blue symbol, 240) has a resulting ϵ_{pp} that is almost double its ϵ_{pp} from the single-molecule parameterization, putting into question the assumption of lateral homogeneity that underpins the experimental analysis for those source data [9], and the third anomalous data point is for non-glycosylated Nup98 (blue symbol, ≈ 500 amino acids) [9] for which the – physiologically relevant – glycosylated version (Nup98-Glyco, black symbol, ≈ 500 amino acids) yields a three times higher film thickness [20]. With these three exceptions, experimental and computational data for $\langle\epsilon_{pp}\rangle_{FG} = 0.5 \pm 0.2 k_B T$ again show close agreement with the predictions for ideal polymers. In the ϵ_{pp} range relevant for FG nups, the computed film thickness (Figure 2c) shows a step change from a swollen polymer film to a nearly fully compacted film, as also indicated by other measures of film compaction, the mass density and file compressibility (where the file compressibility is defined as the information redundancy in a file containing bead coordinates, see methods [31]). The mass density of the FG nups, in the relevant ϵ_{pp} range, is in excellent agreement with the FG nup mass density in the NPC, as estimated using models including finer molecular detail [30].

Interestingly, this change in compaction is even more abrupt (in the relevant ϵ_{pp} range) for FG nups that are assembled in the pore geometry of the NPC, as here probed by MD simulations on NPC-mimetics (NuPODs) based on well-defined numbers and types of FG nups grafted in a DNA origami pore scaffold [32] (Figures S5 and S6). Hence in the physiologically relevant parameter range, we observe that FG nup assemblies can undergo large conformational changes for only minor changes in intermolecular interactions [14, 33], consistent with

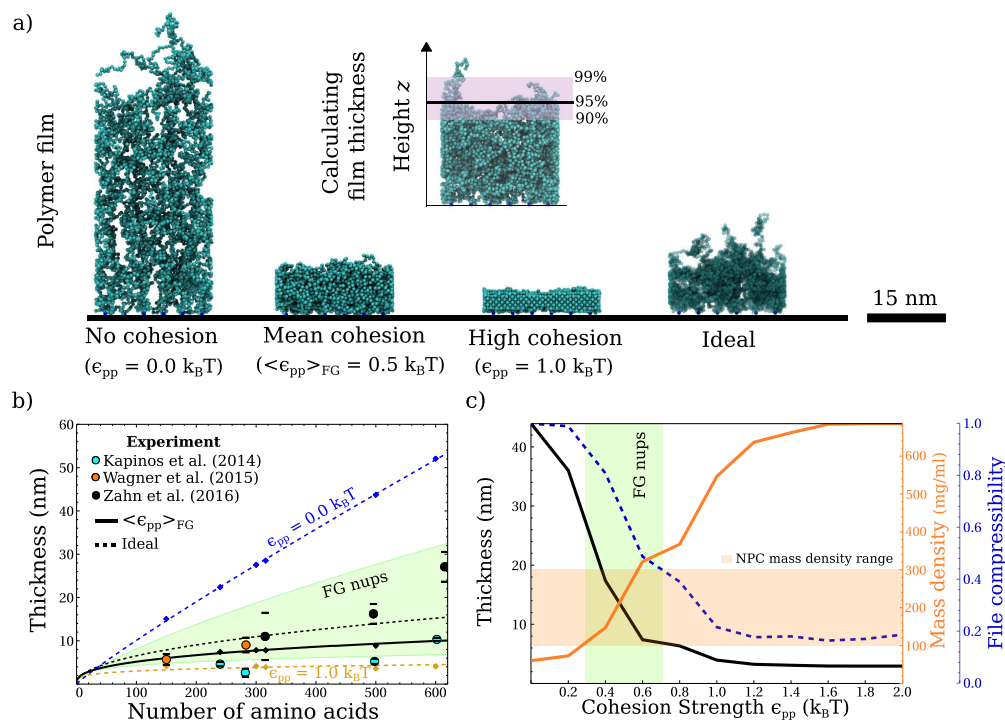


FIG. 2. Validation of the polymer model and inferred cohesion strength (ϵ_{pp}) range through comparison with planar assemblies of FG nups. **a)** MD equilibrated snapshots of polymers ($N = 300$ beads) grafted onto a surface with density 3.2 polymers per 100 nm^2 , *i.e.*, 31 nm^2 per polymer, for various ϵ_{pp} and for the ideal system (no interactions). The inset illustrates the computational definition of the film thickness as the film height containing 95% of the beads. **b)** Experimental film thicknesses (circles) plotted for FG nup domains of different lengths (number of amino acids). MD simulation thicknesses (diamonds) are shown as a function of length for polymers with no cohesion, ideal polymers, polymers with the mean cohesion strength $\langle \epsilon_{pp} \rangle_{FG} = 0.5 \pm 0.2 k_B T$ (green shading), and polymers with high cohesion alongside power law fits. **c)** Measures of compaction for MD simulations as a function of ϵ_{pp} . In the ϵ_{pp} range relevant for FG nups (green shading), the film thickness steeply declines. In this range, the mass density of the FG nup film is consistent with the mass density of FG nups in the NPC [30]. File compressibility (see text and Methods) provides another way of quantifying FG nup compaction.

previous experimental/ computational comparisons for native NPCs [34].

Excluded-volume and cohesive interactions balance to yield ideal polymer behaviour

To further explore the ideal polymer behaviour of FG nups at the crossover from a predominantly entropic brush to a compacted brush dominated by cohesive interactions, we utilized a density functional theory (DFT) in which grafted FG nups are described as ideal polymers interacting with a mean field that is optimized to best represent the net effect of excluded-volume, cohesion, and grafting of the FG nups to an impenetrable surface (see Methods) [14]. This DFT yields film thicknesses of grafted FG nups that are in good agreement with the MD simulations of the same system (Figure S7), and allows us to quantify the effect of molecular interactions via the mean field per polymer in the film (Figure S8). Upon increasing ϵ_{pp} , the mean field energy per polymer, *i.e.*, the product of the mean field per polymer and the density (integrated over the film volume and multiplied by $k_B T$), changes from positive values (a net repulsive interaction), to zero (ideal polymer regime), and finally to negative values (a net cohesive interaction) (Figure 3a). Interestingly, in the ϵ_{pp} range that applies to FG nups, overall interactions remain approximately balanced regardless of changes in the grafting density. For a physiologically relevant grafting density, the magnitude of the mean field energy is only $< 0.5 k_B T$ (per polymer, as before) in the relevant ϵ_{pp} range, and mean field energies for polymers of different lengths appear to all cross at a single point, which coincides with a zero mean field, *i.e.*, ideal polymer behaviour (Figure 3b). We note that the second virial coefficient (see Methods) is close to zero at $\langle \epsilon_{pp} \rangle_{FG} = 0.5 k_B T$, again corresponding to Θ -point, ideal behaviour (Figure 3c) [35]. The Θ -point occurs in other theories that use one essential interaction parameter, for example χ in Flory-Huggins theory, which also leads to a vanishing of the second virial coefficient at this Θ -point [36]. Taken together, we conclude that the (repulsive) excluded-volume and (attractive) cohesive interactions balance, *i.e.*, neither excluded-volume nor cohesion dominates, to yield ideal polymer behaviour for FG nups grafted at physiologically relevant densities (Figure 3d).

FG nups show rapid resealing and fast molecular-scale dynamics

Thus far, we have observed that FG nup morphologies resemble those of ideal polymers, that they are at the transition between two (extreme) regimes of polymer behaviour, and

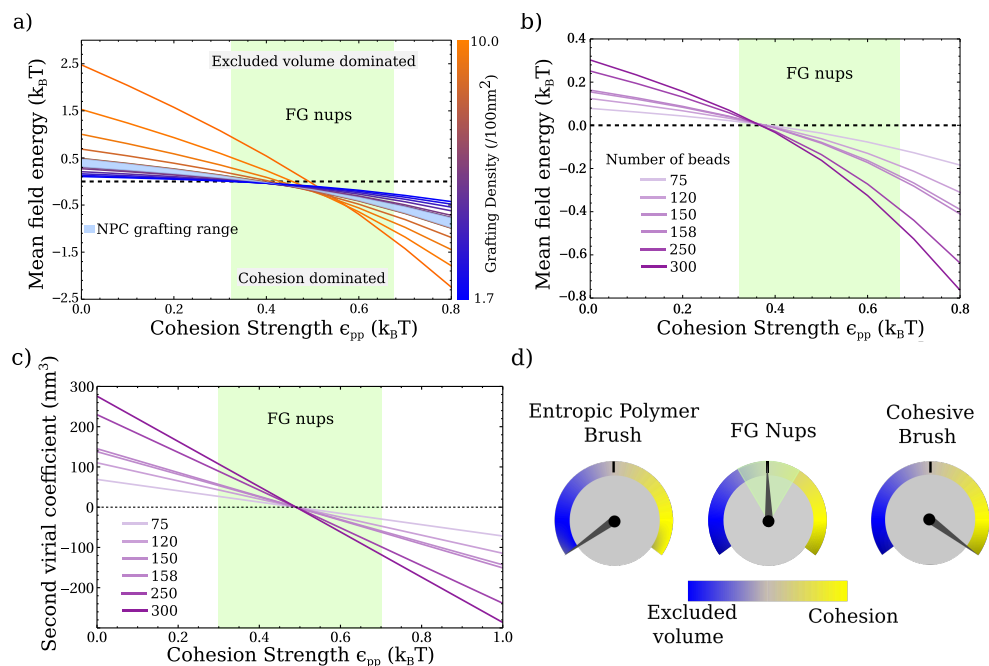


FIG. 3. Planar assemblies of FG nups adopt morphologies that balance excluded-volume and cohesive interactions analysed by DFT. **a)** The mean field energy per polymer as a function of ϵ_{pp} for a range of grafting densities ($N = 300$ beads, equivalent to 600 amino acids). **b)** The mean field energy per polymer for various polymer lengths, for planar assemblies with a physiological grafting density of 3.2 polymers per 100 nm^2 (31 nm^2 per polymer). **c)** The second virial coefficient as a function of ϵ_{pp} calculated from the bead pair potential (see Methods). **d)** An illustration of the overall balance between excluded-volume and cohesive interactions for FG nup planar assemblies, causing the FG nup behaviour to be in between predictions for an entropic polymer brush, with molecular interactions predominantly due to excluded-volume, and for a compacted brush, with predominantly cohesive molecular interactions.

that at this transition, it is possible to have large conformational changes for small changes in molecular interactions. This latter observation appears to be of significant physiological relevance, as it provides a mechanism by which FG nup assemblies in the NPC may open and close [14] to facilitate transport of large cargoes at millisecond time scales without compromising the transport barrier. Using MD simulations, we also probed the resealing dynamics of the barrier, *i.e.*, how fast and by how much polymers fill the center of the pore following the creation of holes (void of polymers) of 10, 20, and 30 nm diameter in a NuPOD pore system containing 48 polymers [32] (Figure 4a and Figure S9). We observe

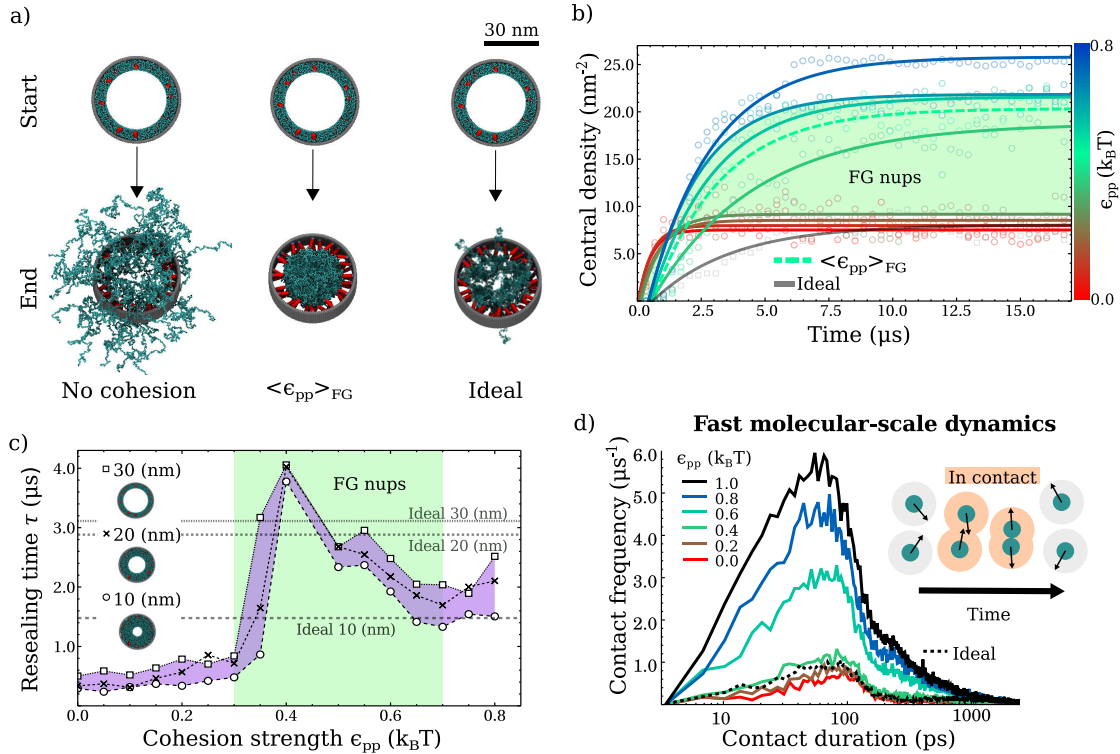


FIG. 4. FG nups exhibit rapid dynamics on both the mesoscale and molecular scale. **a)** *In silico* resealing experiments on NPC mimics [32] begin with a (30 nm diameter) hole, void of polymers, in the pore followed by the release of the polymers. The arrow represents 34 μs (or 10^7 timesteps) of simulation time, pointing to snapshots of the resulting, equilibrated, polymer conformations. **b)** The number of beads in a circular cross-sectional area with 5 nm radius located at the pore centre, versus time. Data points were taken every 0.34 μs . The cohesion strength colour bar represents the range $\epsilon_{pp} = (0.0, 0.1, 0.2, 0.3, 0.4, 0.5, 0.6, 0.7, 0.8) k_B T$. Lines represent fits to the function $\rho(t) = \rho_{max}(1 - \exp(-t/\tau))$ where ρ_{max} is the maximum areal density and τ defines the resealing time. **c)** The resealing time as a function of ϵ_{pp} , for different hole diameters. Horizontal dashed lines indicate the respective resealing times for the ideal polymer case. **d)** Distribution of contact durations for a single isolated polymer ($N = 300$ beads). Simulations were run for 0.34 μs and configurations were analysed every $3.4 \times 10^{-6} \mu\text{s}$.

that FG nup resealing of the pore can be characterized by two regimes depending on the cohesion strength ϵ_{pp} (Figure 4b,c). For $\epsilon_{pp} \gtrsim 0.4 k_B T$, the centre of the pore reaches a maximum polymer density that is approximately double that for $\epsilon_{pp} < 0.4 k_B T$. We also observe that for $\epsilon_{pp} \gtrsim 0.4 k_B T$, the resealing rate appears slower than for $\epsilon_{pp} < 0.4 k_B T$,

where polymers rapidly extend away from their tethering points (Figure S9). To further investigate the resealing rate, we probe the resealing time, τ , which is the time taken for the central density to reach $\approx 63\%$ its equilibrium value (Figure 4c). Notably, for polymers with $\epsilon_{pp} = \langle \epsilon_{pp} \rangle_{FG} = 0.5 k_B T$, the resealing time for “large cargoes” (10–30 nm diameter) is similar to that of ideal polymers (defined as before, by the absence of intermolecular interactions), albeit that the central density remains at a relatively low level for the ideal polymer case. This implies that the similarity to ideal polymers also extends to the dynamic behaviour of FG nups. Typically, the resealing times are on the microsecond time-scale, which is much faster – as needed to inhibit unspecific transport – than the millisecond time scale as reported for transport events, and in agreement with previous simulations [37]. We also observe a sharp transition in resealing time occurring at $0.3 k_B T < \epsilon_{pp} < 0.4 k_B T$, which falls in the relevant ϵ_{pp} range as inferred from experiments on single FG nup constructs.

Finally, we investigate how the cohesive interactions between FG nups affect dynamics at molecular and submolecular length scales. Of note, nuclear magnetic resonance spectroscopy indicates fast (on the picosecond - nanosecond time scale) FG nup residue dynamics [38, 39], presumably indicative of entropically dominated FG nup behaviour. We therefore simulated free, single polymers (in the absence of other polymers) in thermodynamic equilibrium and measured the durations of bead-bead contacts, *i.e.*, the elapsed time during which the centres of adjacent beads (excluding bonded neighbours on a chain) are within the range of the attractive pair potential, (Figure 4d). Of note, the relevant time scales appear rather independent of ϵ_{pp} . This may appear counterintuitive given the strong dependence of the *collective* FG nup morphology on ϵ_{pp} (Figures 1, 2), but can be explained as due to the weakness of the *individual* bead-bead interactions. On the other hand, the number of contacts increases with ϵ_{pp} , which can be attributed to the higher local bead concentration for larger ϵ_{pp} . Overall, individual FG nups exhibit fast dynamics (picosecond time-scale) at (sub-)molecular length scales, characteristic of their entropic nature. At larger length scales FG nup assemblies, dominated by the collective FG nup molecular interactions, exhibit microsecond dynamics with enhanced resealing (due to cohesion) which is of sufficient speed and efficiency to maintain the transport barrier.

CONCLUSION

In summary, we find that the behaviour of FG nup assemblies is not governed by (repulsive) excluded-volume interactions, characterized as ‘entropic polymer brush’ behaviour, nor by (attractive) cohesive interactions, but by being at the crossover of these two extreme regimes. That is, the FG nups can be characterized by the balance of repulsive and cohesive molecular interactions, *i.e.*, the FG nups are at or close to their Θ -point in physiological buffer solutions. This leads to ideal polymer behaviour, as evidenced by the adopted FG nup morphologies and from their resealing dynamics following perturbation. In this regime, the morphology of FG nups, grafted at physiological densities, has increased sensitivity to small changes in cohesion strength. As a consequence, the morphology of the FG nups can be readily modulated, *e.g.*, towards more compact arrangements aided by nuclear transport receptors [9, 22, 40–42] or towards more dilute arrangements due to generic crowding in the cell [38, 43]. In the physiological context, this suggests a mechanism to facilitate the collective FG nup rearrangements that are needed for transport of large cargoes through the NPC. In addition, the rapid movement of FG nups on the molecular scale — maintained through a large range of cohesion strengths — will facilitate the uptake and release of nuclear transport factors and associated cargoes [44], whereas the accumulation of many weakly cohesive interactions facilitates the tight sealing of the NPC transport barrier, maintained by FG nup condensation.

ACKNOWLEDGEMENTS

We thank Dino Osmanović (MIT), Roy Beck (Tel-Aviv), Larissa Kapinos (Basel), Roderick Lim (Basel) and Anton Zilman (Toronto) for helpful discussions; and the Institute for physics of living systems (UCL IPLS) for computational resources. This work was funded by the UK Engineering and Physical Sciences Research Council (EPSRC, EP/L504889/1).

AUTHOR CONTRIBUTIONS

L.K.D. and B.W.H. conceived the study and designed the polymer model. L.K.D., B.W.H., and A.S. planned the simulations. L.K.D. performed the simulations, analysed the simulation data, analysed external experimental data, and made the figures. I.J.F. ad-

vised on the DFT calculations. A.S. advised on the LAMMPS (MD) simulations. L.K.D. and B.W.H. wrote the manuscript. All authors interpreted the results and commented on the manuscript.

-
- [1] Jovanovic-Talisman T, Zilman A (2017) Protein Transport by the Nuclear Pore Complex: Simple Biophysics of a Complex Biomachine. *Biophys. J.* 113(1):6–14.
 - [2] Aramburu IV, Lemke EA (2017) Floppy but not sloppy: Interaction mechanism of FG-nucleoporins and nuclear transport receptors. *Semin. Cell Dev. Biol.* 68:34–41.
 - [3] Stanley GJ, Fassati A, Hoogenboom BW (2017) Biomechanics of the transport barrier in the nuclear pore complex. *Semin. Cell Dev. Biol.* 68:42–51.
 - [4] Hülsmann BB, Labokha AA, Görlich D (2012) The permeability of reconstituted nuclear pores provides direct evidence for the selective phase model. *Cell* 150(4):738–751.
 - [5] Yamada J, et al. (2010) A Bimodal Distribution of Two Distinct Categories of Intrinsically Disordered Structures with Separate Functions in FG Nucleoporins. *Mol. Cell. Proteomics* 9(10):2205–2224.
 - [6] Denning DP, Patel SS, Uversky V, Fink AL, Rexach M (2003) Disorder in the nuclear pore complex: The FG repeat regions of nucleoporins are natively unfolded. *Proc. Natl. Acad. Sci.* 100(5):2450–2455.
 - [7] Lim RY, et al. (2007) Nanomechanical basis of selective gating by the nuclear pore complex. *Science.* 318(5850):640–643.
 - [8] Schoch RL, Kapinos LE, Lim RYH (2012) Nuclear transport receptor binding avidity triggers a self-healing collapse transition in FG-nucleoporin molecular brushes. *Proc. Natl. Acad. Sci.* 109(42):16911–16916.
 - [9] Kapinos LE, Schoch RL, Wagner RS, Schleicher KD, Lim RYH (2014) Karyopherin-centric control of nuclear pores based on molecular occupancy and kinetic analysis of multivalent binding with FG nucleoporins. *Biophys. J.* 106(8):1751–1762.
 - [10] Timney BL, et al. (2016) Simple rules for passive diffusion through the nuclear pore complex. *J. Cell Biol.* 215(1):57–76.
 - [11] Labokha AA, et al. (2013) Systematic analysis of barrier-forming FG hydrogels from *Xenopus* nuclear pore complexes. *EMBO J.* 32(2):204–218.

- [12] Schmidt HB, Görlich D (2015) Nup98 FG domains from diverse species spontaneously phase-separate into particles with nuclear pore-like permselectivity. *Elife* 4:e04251.
- [13] Peleg O, Tagliazucchi M, Kröger M, Rabin Y, Szleifer I (2011) Morphology control of hairy nanopores. *ACS Nano* 5(6):4737–4747.
- [14] Osmanovic D, et al. (2012) Bistable collective behavior of polymers tethered in a nanopore. *Phys. Rev. E - Stat. Nonlinear, Soft Matter Phys.* 85(6):1–8.
- [15] Eisele NB, Labokha AA, Frey S, Görlich D, Richter RP (2013) Cohesiveness tunes assembly and morphology of FG nucleoporin domain meshworks - Implications for nuclear pore permeability. *Biophys. J.* 105(8):1860–1870.
- [16] Osmanovic D, Rabin Y (2018) Effect of Grafting on Aggregation of Intrinsically Disordered Proteins. *Biophys. J.* 114(3):534–538.
- [17] Gamini R, Han W, Stone JE, Schulten K (2014) Assembly of Nsp1 Nucleoporins Provides Insight into Nuclear Pore Complex Gating. *PLoS Comput. Biol.* 10(3):e1003488.
- [18] Ghavami A, Van der Giessen E, Onck PR (2018) Sol–gel transition in solutions of FG-Nups of the nuclear pore complex. *Extrem. Mech. Lett.* 22:36–41.
- [19] Vovk A, et al. (2016) Simple biophysics underpins collective conformations of the intrinsically disordered proteins of the Nuclear Pore Complex. *Elife* 5:e10785.
- [20] Zahn R, et al. (2016) A physical model describing the interaction of nuclear transport receptors with FG nucleoporin domain assemblies. *Elife* 5:e14119.
- [21] Denning DP, Uversky V, Patel SS, Fink AL, Rexach M (2002) The *Saccharomyces cerevisiae* nucleoporin Nup2p is a natively unfolded protein. *J. Biol. Chem.* 277(36):33447–33455.
- [22] Wagner RS, Kapinos LE, Marshall NJ, Stewart M, Lim RYH (2015) Promiscuous binding of karyopherin β 1 modulates FG nucleoporin barrier function and expedites NTF2 transport kinetics. *Biophys. J.* 108(4):918–927.
- [23] Lim RYH, et al. (2006) Flexible phenylalanine-glycine nucleoporins as entropic barriers to nucleocytoplasmic transport. *Proc. Natl. Acad. Sci.* 103(25):9512–9517.
- [24] Stirnemann G, Giganti D, Fernandez JM, Berne BJ (2013) Elasticity, structure, and relaxation of extended proteins under force. *Proc. Natl. Acad. Sci.* 110:3847–3852.
- [25] Ghavami A, van der Giessen E, Onck PR (2012) Coarse-grained potentials for local interactions in unfolded proteins. *J. Chem. Theory Comput.* 9(1):432–440.

- [26] de. Gennes PG (1979) *Scaling concepts in polymer physics*. (Cornell University Press, Ithaca, NY).
- [27] Wilkins D, et al. (1999) Hydrodynamic radii of native and denatured proteins measured by pulse field gradient NMR techniques. *Biochemistry* 38:16424–164431.
- [28] Choi UB, McCann JJ, Weninger KR, Bowen ME (2011) Beyond the random coil: Stochastic conformational switching in intrinsically disordered proteins. *Structure* 19(4):566–576.
- [29] Ladd AJ, Frenkel D (1992) Computer Simulation Studies of Static and Dynamical Scaling in Dilute Solutions of Excluded-Volume Polymers. *Macromolecules* 25(13):3435–3438.
- [30] Ghavami A, Veenhoff LM, Van Der Giessen E, Onck PR (2014) Probing the disordered domain of the nuclear pore complex through coarse-grained molecular dynamics simulations. *Biophys. J.* 107(6):1393–1402.
- [31] Avinery R, Kornreich M, Beck R (2018) Universal and efficient entropy estimation using a compression algorithm. *arXiv:1709.10164v3*.
- [32] Fisher PDE, et al. (2018) A Programmable DNA Origami Platform for Organizing Intrinsically Disordered Nucleoporins within Nanopore Confinement. *ACS Nano* 12(2):1508 – 1518.
- [33] Ro S, Gopinathan A, Kim YW (2018) Interactions between a fluctuating polymer barrier and transport factors together with enzyme action are sufficient for selective and rapid transport through the nuclear pore complex. *Phys. Rev. E* 98(012403):1–14.
- [34] Bestembayeva A, et al. (2015) Nanoscale stiffness topography reveals structure and mechanics of the transport barrier in intact nuclear pore complexes. *Nat. Nanotechnol.* 10(1):60–64.
- [35] Sheng YJ, Panagiotopoulos AZ, Kumar SK, Szleifer I (1994) Monte Carlo Calculation of Phase Equilibria for a Bead-Spring Polymeric Model. *Macromolecules* 27(2):400–406.
- [36] Williams C, Brochard F, Frisch HL (1981) Polymer Collapse. *Annu. Rev. Phys. Chem.* 32:433–451.
- [37] Moussavi-Baygi R, Mofrad MR (2016) Rapid Brownian Motion Primes Ultrafast Reconstruction of Intrinsically Disordered Phe-Gly Repeats Inside the Nuclear Pore Complex. *Sci. Rep.* 6(29991):1–12.
- [38] Hough LE, et al. (2015) The molecular mechanism of nuclear transport revealed by atomic-scale measurements. *Elife* 4:e10027.
- [39] Milles S, et al. (2015) Plasticity of an Ultrafast Interaction between Nucleoporins and Nuclear Transport Receptors. *Cell* 163(3):734–745.

- [40] Yang W, Musser SM (2006) Nuclear import time and transport efficiency depend on Importin β concentration. *J. Cell Biol.* 174(7):951–961.
- [41] Jovanovic-Talisman T, et al. (2009) Artificial nanopores that mimic the transport selectivity of the nuclear pore complex. *Nature* 457(7232):1023–1027.
- [42] Lowe AR, et al. (2015) Importin- β modulates the permeability of the nuclear pore complex in a Ran-dependent manner. *Elife* 4:e04052.
- [43] Tetenbaum-Novatt J, Hough LE, Mironska R, McKenney AS, Rout MP (2012) Nucleocytoplasmic Transport: A Role for Nonspecific Competition in Karyopherin-Nucleoporin Interactions. *Mol. Cell. Proteomics* 11(5):31–46.
- [44] Hayama R, et al. (2018) Thermodynamic characterization of the multivalent interactions underlying rapid and selective translocation through the nuclear pore complex. *J. Biol. Chem.* 293:4555–4563.